The impact of spike-frequency adaptation on balanced network dynamics

Victor J. Barranca, Han Huang & Sida Li

Cognitive Neurodynamics

ISSN 1871-4080

Cogn Neurodyn
DOI 10.1007/s11571-018-9504-2

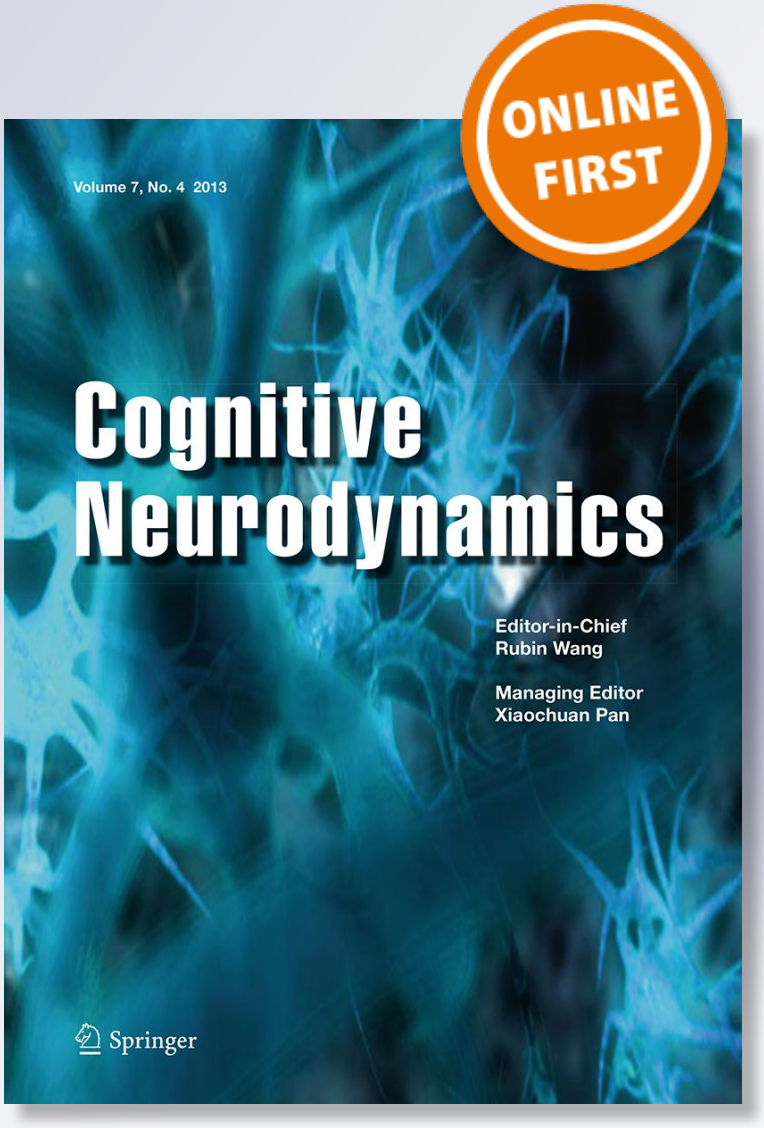

Springer

Cognitive Neurodynamics
https://doi.org/10.1007/s11571-018-9504-2

RESEARCH ARTICLE

The impact of spike-frequency adaptation on balanced network dynamics

Victor J. Barranca[1] · Han Huang[1] · Sida Li[1]

Received: 20 March 2018 / Revised: 20 July 2018 / Accepted: 28 August 2018

Abstract
A dynamic balance between strong excitatory and inhibitory neuronal inputs is hypothesized to play a pivotal role in information processing in the brain. While there is evidence of the existence of a balanced operating regime in several cortical areas and idealized neuronal network models, it is important for the theory of balanced networks to be reconciled with more physiological neuronal modeling assumptions. In this work, we examine the impact of spike-frequency adaptation, observed widely across neurons in the brain, on balanced dynamics. We incorporate adaptation into binary and integrate-and-fire neuronal network models, analyzing the theoretical effect of adaptation in the large network limit and performing an extensive numerical investigation of the model adaptation parameter space. Our analysis demonstrates that balance is well preserved for moderate adaptation strength even if the entire network exhibits adaptation. In the common physiological case in which only excitatory neurons undergo adaptation, we show that the balanced operating regime in fact widens relative to the non-adaptive case. We hypothesize that spike-frequency adaptation may have been selected through evolution to robustly facilitate balanced dynamics across diverse cognitive operating states.

Keywords Spike-frequency adaptation · Balanced networks · Neuronal network models · Nonlinear dynamics

Introduction

There is strong experimental evidence that individual neurons across the brain demonstrate highly irregular and asynchronous firing activity, but the basis for this variability remains a subject of intense investigation (Shadlen and Newsome 1998b; Britten et al. 1993; London et al. 2010; Compte et al. 2003). This irregular activity facilitates rich neuronal network computations and has been shown to foster predictive neuronal coding, efficient representation of stimuli, and effective short-term memory (Shadlen and Newsome 1998a; Sussillo and Abbott 2009; Whalley 2013). Considering biophysical sources of noise are largely unable to account for irregular neuronal dynamics (Softky and Koch 1993; Faisal et al. 2008), there is robust evidence that neuronal network topology and strong neuronal interaction together are sufficient to give rise to the irregular activity observed in vivo even in the absence of variability in external network inputs.

The theory of *balanced networks* indicates the existence of an irregular operating regime in which strong excitatory and inhibitory neuronal inputs are dynamically balanced, typically rendering neurons in a near-firing state such that firing events are caused by fluctuations in neuronal input (van Vreeswijk and Sompolinsky 1996; Troyer and Miller 1997; Vogels and Abbott 2005; Miura et al. 2007). Theoretical analysis of the balanced operating state demonstrates that when temporal fluctuations in neuronal input are approximately as strong as the mean input, neuronal firing rates in a balanced network are broadly distributed while maintaining asynchronous dynamics and nearly constant population-averaged activity. Supporting the existence of a balanced state in physical neuronal networks, experimental studies indicate that in several brain regions excitatory and inhibitory inputs are indeed closely tracked over time, with the ratio of excitatory to inhibitory conductances remaining nearly constant both in vivo and in vitro (Wehr and Zador 2003; Shu et al. 2003; Atallah and Scanziani 2009; Xue et al. 2014).

✉ Victor J. Barranca
vbarran1@swarthmore.edu

[1] Swarthmore College, 500 College Avenue, Swarthmore, PA 19081, USA

Published online: 03 September 2018

Crucial to the robustness of the theory of balanced networks is that it generalizes to both experimental settings and detailed neuronal network models. Neuronal network models demonstrating balanced dynamics are generally sparsely connected and exhibit relatively strong synaptic connections, which are characteristics well supported physiologically (Markram et al. 1997; Mason et al. 1991; He et al. 2007; Achard and Bullmore 2007; Destexhe et al. 2003), but current theoretical work largely utilizes minimal single neuron models for analytical tractability in studying the persistence of balanced dynamics (Boerlin et al. 2013; Litwin-Kumar and Doiron 2012; Mongillo et al. 2012; Renart et al. 2010; Deneve and Machens 2016). In examining the robustness of the balanced network theory, a question that naturally arises is whether balanced dynamics are preserved in the face of more realistic neuronal modeling assumptions.

One salient feature of single neuron dynamics found widely across the brain is a decrease in firing rate over time in response to a constant stimulus known as *spike-frequency adaptation* (Brown and Adams 1980; Benda and Herz 2003; Barranca et al. 2014a). Spike-frequency adaptation may serve a number of significant functional roles, particularly in stimulus selection, decision making, and population coding (Benda et al. 2005; Peron and Gabbiani 2009; Kilpatrick and Ermentrout 2011), and has profound consequences on the dynamical characteristics of neurons, including their bifurcation structure and bursting propensity (van Vreeswijk and Hansel 2001; Stiefel et al. 2009).

To examine the robustness of the balanced network theory and further characterize the implications of spike-frequency adaptation, we examine the existence of the balanced state in neuronal network models incorporating spike-frequency attenuation. Our work shows that when the entire neuronal network undergoes adaptation, balanced dynamics persist even for moderately strong adaptation. Using mean-field analysis and a long-time approximation of the model dynamics, we derive theoretical bounds on the network parameters necessary for balanced dynamics, highlighting the impact of adaptation strength on the parameter regime in which neuronal dynamics are balanced. We also perform an exhaustive exploration of the adaptation parameter space, investigating several relevant metrics of balance as a function of adaptation strength. For concreteness, we initially examine a binary network model (van Vreeswijk and Sompolinsky 1996), and later demonstrate how our analysis generalizes to a pulse-coupled integrate-and-fire (I&F) network model (Corral et al. 1995; Mather et al. 2009; Barranca et al. 2014b).

This work shows that the balanced state theory is indeed consistent with more realistic neuronal dynamics, underlining a generalizable framework for potential verification of balanced dynamics in novel neuronal models. Importantly, we show that in the case when only the excitatory neuron population demonstrates spike-frequency attenuation, balanced dynamics are preserved for strong adaptation well above the strength generally observed in vivo and for a broader range of model parameters. This result is consistent with experimental evidence that excitatory neurons are generally more likely to undergo adaptation than inhibitory neurons (La Camera et al. 2006; Augustin et al. 2013). We therefore conjecture that adaptation in excitatory neurons may in fact function as a potential mechanism for fostering balanced dynamics among neuronal populations.

The remainder of the paper is organized as follows. We first formulate the binary network model incorporating spike-frequency adaptation in the "Binary model with spike-frequency adaptation" section and then we perform mean-field analysis on the model in the "Mean-field analysis" section, deriving conditions on the neuronal inputs in the large network and long time limits necessary for balanced dynamics. In the "Theoretical bounds on balanced dynamics" section, we derive theoretical bounds on the model parameters required for balanced activity, analyzing in detail the specific impact of adaptation strength. We also consider the physiological case in which only the excitatory population undergoes adaptation in the "Adaptation exclusively in excitatory population" section, demonstrating adaptation broadens the parameter regime over which the dynamics are balanced. In the "Numerical investigation of spike-frequency adaptation" section, we numerically investigate the spike attenuation parameter space and its impact on the model network dynamics, generalizing these results to integrate-and-fire network models with adaptation in the "Generalization to integrate-and-fire model" section. Finally, in the "Discussion" section, we discuss our findings, their implications, and potential related areas of future investigation.

Binary model with spike-frequency adaptation

We first introduce spike-frequency adaptation into the framework of a binary neuronal model analogous to the Ising model of ferromagnetism in statistical mechanics (Glauber 1963; van Vreeswijk and Sompolinsky 1996). As the name suggests, in this model each neuron has two major states, firing ($\sigma = 1$) or quiescent ($\sigma = 0$). The network is composed of N neurons, such that N_E are excitatory and N_I are inhibitory, requiring that for balanced dynamics these two subpopulations interact such that firing events are largely the result of input fluctuations of strength comparable to the mean input. The state of the ith neuron in the kth population at time t is prescribed by the below

dynamical system (subscripts $k = E$ and $k = I$ denote excitatory and inhibitory neurons, respectively)

$$\sigma_k^i(t) = H\big(\mu_k^i(t) - \theta_k^i(t)\big), \tag{1}$$

where $H(\cdot)$ denotes the Heaviside function, $\mu_k^i(t)$ is the total input into the neuron at time t, and $\theta_k^i(t)$ is the firing threshold for the ith neuron in the kth population at time t. The total synaptic drive into the ith neuron in the kth population at time t is

$$\mu_k^i(t) = \sum_{j=1}^{N_E} R_{kE}^{ij}\sigma_E^j(t) + \sum_{j=1}^{N_I} R_{kI}^{ij}\sigma_I^j(t) + \mu_k^0, \tag{2}$$

where R_{kl}^{ij} denotes the recurrent connection strength between the ith post-synaptic neuron in the kth population and the jth pre-synaptic neuron in the lth population and μ_k^0 is the strength of the external input into the kth population. Note that the state of the neurons are updated sequentially using a fixed step-size in numerical simulation of this discrete dynamical system and only state transitions from quiescent to firing are considered novel firing events. The state space reflects only the neuronal firing dynamics, which encode the essential information for determining balanced dynamics, whereas the more physiological integrate-and-fire model analyzed in the "Generalization to integrate-and-fire model" section also reflects the subthreshold voltage dynamics.

To incorporate spike-frequency adaptation, we include in our modeling framework a dynamic firing threshold for each neuron rather than a static population-based firing threshold as in classical balanced network theory. This dynamic firing threshold increases the neuronal excitation necessary for an action potential, with the impact of multiple subsequent spikes adding over time to yield an accumulated increase in firing threshold and thus a cumulatively reduced firing frequency. From a physiological perspective, there are two primary slow currents that promote spike-frequency attenuation through slow negative feedback to the neuronal excitability. The first is the non-inactivating muscarinic potassium current and the second is the after-hyperpolarization (AHP) current, which together largely determine the spike threshold and slope of the neuronal voltage trace (Ermentrout et al. 2001; Yamada et al. 1989). During an action potential, a large number of voltage-gated and calcium-dependent ionic channels open, facilitating a sharp rise in the adaptation currents passing through the neuron. As these adaptation currents slowly deactivate, their impact builds over time following additional firing events and thereby reduces the neuronal spike frequency.

The use of a dynamic firing threshold in modeling spike-frequency adaptation is ubiquitous in neuronal models, generating negative correlations between the durations of successive inter-spike intervals and reproducing adaptive neuronal firing dynamics observed in vivo (Treves 1993; Bibikov and Ivanitski 1985; Chacron et al. 2000; Kobayashi 2009; Kobayashi and Kitano 2016). Alternative models of spike attenuation instead directly incorporate the dynamics of the slow adaptation currents into the subthreshold voltage activity (Benda et al. 2010; Barranca et al. 2014a; Fourcaud-Trocme et al. 2003; Liu and Wang 2001). Hence, to study the impact of spike-frequency adaptation on balanced dynamics in the context of the binary neuron model, which focuses on firing activity only, we introduce a dynamic firing threshold to reflect adaptation, and since the integrate-and-fire neuron modeling framework incorporates subthreshold voltage activity as well as firing dynamics, in the "Generalization to integrate-and-fire model" section we also investigate the dynamics of a current-based adaptation model. We observe strong qualitative agreement in the effect of spike-frequency adaptation on balanced dynamics using the two modeling frameworks.

Building upon the state space dynamics of the network model given by Eqs. (1) and (2), the dynamic firing threshold $\theta_k^i(t)$ for the ith neuron in the kth population evolves discretely according to

$$\theta_k^i(t) = \theta_k + \big(\theta_k^i(t_0) - \theta_k + \phi F(\mu_k^i(t))\big)e^{-\lambda(t-t_0)}, \tag{3}$$

where θ_k denotes the constant non-adapted firing threshold for all neurons in the kth population, $F(\cdot)$ denotes the firing event indicator function, and t_0 refers to the closest preceding time at which the neuron fired. The firing threshold for a given neuron in the kth population increases instantaneously by jump strength ϕ each time it undergoes an action potential, and the adaptation offset from default threshold θ_k decreases exponentially in time with rate determined by λ. The overall adaptation strength thereby increases with jump strength ϕ and decreases with decay rate λ, and a quotient of these two parameters, for example, could be used to quantify the adaptation strength. Thus, for sufficiently slow decay in the firing threshold, several succeeding firing events will result in a cumulative increase in the firing threshold. However, in the absence of firing events, a neuronal firing threshold will approach its non-adapted threshold.

In prescribing the network architecture, we select connection strength R_{kl}^{ij} to be $R_{kl}/\sqrt{K}$ with probability K/N_l and 0 otherwise, ignoring any detailed network structure to mechanistically focus on the impact of the single neuron dynamics. In this case, the excitatory connection strength $R_{kE} > 0$ and the inhibitory connection strength $R_{kI} < 0$. Assuming sparse connectivity, where $1 \ll K \ll N_E, N_I$, each neuron receives on average K excitatory incoming connections and K inhibitory incoming connections. Therefore, if R_{kl} is $\mathcal{O}(1)$, then only $\mathcal{O}(\sqrt{K})$ excitatory inputs are necessary for a neuron to fire given an $\mathcal{O}(1)$

firing threshold, reflecting strong recurrent connectivity as in classical balanced network theory (van Vreeswijk and Sompolinsky 1996). When the mean excitatory and inhibitory inputs into each neuron are in summation of the same order as the firing threshold, intermittent fluctuations in input are typically responsible for firing events and also their strongly irregular distribution. We derive conditions for balanced dynamics under these modeling assumptions in the "Theoretical bounds on balanced dynamics" section. As the absolute scale of the neuronal input is inconsequential in this nondimensional model, we assume connectivity parameters $R_{EE} = R_{IE} = 1$, so the only parameters that determine the inhibition relative to excitation are the inhibitory connection strengths and external input. We also use the notation $R_E = |R_{EI}|$ and $R_I = |R_{II}|$ to quantify the magnitude of the inhibitory connections.

In requiring that irregular firing activity is the product only of interactions among neurons in the network, we assume the external input is constant and with strength determined by parameter m_0. Specifically, the constant external input into each population is $\mu_E^0 = Em_0\sqrt{K}$ and $\mu_I^0 = Im_0\sqrt{K}$, where E and I are $\mathcal{O}(1)$ positive parameters controlling the net external input into the excitatory and inhibitory populations, respectively.

Before analyzing the impact of spike-frequency adaptation, for contrast, we first summarize several *main dynamical features* of a neuronal network in the balanced operating regime. As depicted in Fig. 1a, for a representative neuron in a balanced network, the total excitatory and inhibitory inputs are much larger in magnitude than the firing threshold, but the two input types dynamically cancel over time, leaving the total input only irregularly crossing threshold. *This irregular spiking activity with strong excitatory and inhibitory inputs dynamically counteracting produces a nearly constant level of asynchronous neuronal activity across the network*, together characterizing the key features of the balanced state considered in this work. We will later use these key features as a means of benchmarking the degree to which a network with spike-frequency adaptation is balanced.

On a network level, the population-averaged state, or the *mean activity*, for the kth population $m_k(t) = \frac{1}{N_k}\sum_{i=1}^{N_k} \sigma_k^i(t)$ is nearly constant and far below 1 across time, demonstrating irregular fluctuations with small temporal standard deviation about the time-averaged mean activity m_k. Across the network, the variance of the inter-spike intervals is larger than the mean inter-spike interval, signifying irregular firing activity. Thus, a nearly stationary and asynchronous balanced state is achieved, as demonstrated in Fig. 1b. Similarly, for each neuron in the network, the time-averaged ratio between the total excitatory and total inhibitory input into each neuron, which we will refer to as

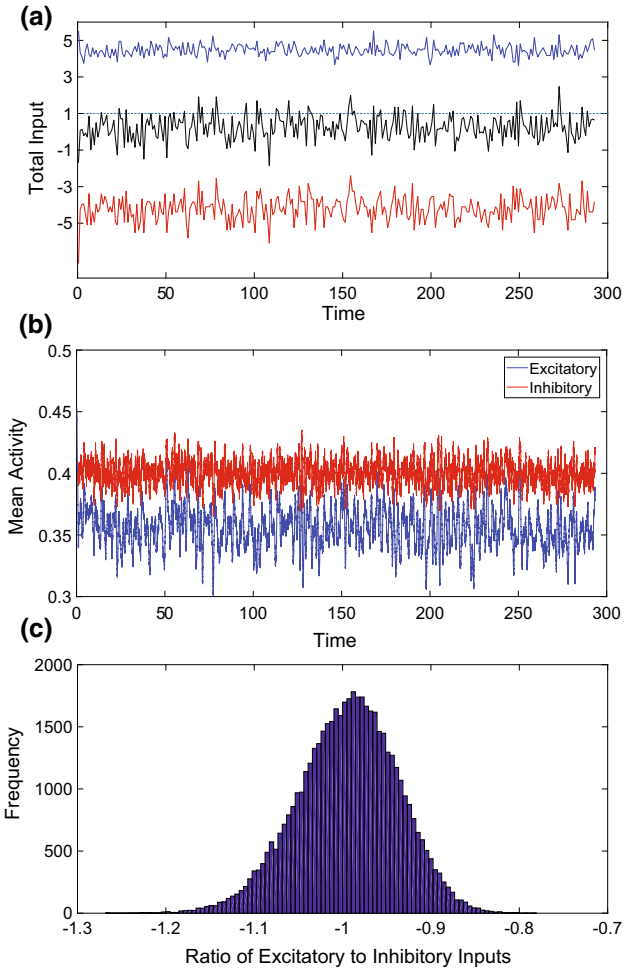

Fig. 1 Dynamics of binary neurons in the balanced operating regime. **a** Excitatory (blue) and inhibitory (red) input into a sample neuron in the balanced state. The total input (black) is dynamically balanced over time, leaving the net input near threshold (dashed). **b** The population-averaged state (mean activity) of each neuron population over time. The mean activity is nearly constant with irregular fluctuations and small temporal variance. **c** Histogram of the ratio between time-averaged excitatory and inhibitory inputs across the neuronal network. The excitatory and inhibitory inputs are primarily proportional, yielding a mean EI ratio near -1. Parameters are chosen such that $N = 5000, N_E = 4000, N_I = 1000, K = 200, E = 1, I = 0.8, R_{EE} = R_{IE} = 1, R_{II} = -1.8, R_{EI} = -2, m_0 = 0.5, \theta_E = 1,$ and $\theta_I = 0.8$. (Color figure online)

the *EI ratio*, is primarily near -1. This indicates that on a neuron-by-neuron basis the excitatory and inhibitory inputs are nearly proportional and consequently well-balanced such that the total input into each neuron is near threshold. A histogram of the EI ratios across a balanced network is given in Fig. 1c. In this network, the ratio of excitatory to inhibitory neurons is chosen to be 4 : 1 in accordance with estimates in the primary visual cortex (Liu 2004; Gilbert 1992), and the remaining network parameter choices are listed in the caption of Fig. 1. It is important to note that

our analysis is largely not sensitive to the ratio of excitatory to inhibitory neurons as well as perturbations in specific parameter choices so long as they are in the subsequently derived theoretical bounds.

Mean-field analysis

We now analytically examine the parameter regime for which binary networks with spike-frequency adaptation demonstrate balanced dynamics. A natural theoretical requirement for a balanced operating state is that in the large network limit the mean activity for both the excitatory and inhibitory populations remains positive and less than 1, implying the mean activity is constant with asynchronous dynamics. Hence, we require $0<m_k<1$ as $N\to\infty$ and as $K\to\infty$ for fixed ratios N_E/N_I and K/N. This requirement ultimately gives theoretical bounds on the parameter space yielding balanced dynamics independent of a specific network size in practice, requiring that a particular finite network realization is composed of a sufficiently large number of interconnected excitatory and inhibitory neurons for these bounds to apply approximately.

While in the absence of adaptation, this analysis is given in van Vreeswijk and Sompolinsky (1998), in the case of our adaptive binary model, we now must account for the dynamic nature of each individual neuronal firing threshold. Based on the requirement of stationarity, we assume that when the network is in a balanced operating regime, in the long-time limit the time-averaged mean activity of each population is constant, given by m_{k_∞} for the kth population, and similarly require that the long-time, time-averaged mean threshold for the kth population, denoted θ_{k_∞}, is constant.

To approximate θ_{k_∞}, we first observe using inductive reasoning that we may compute the firing threshold for the ith neuron in the kth population after n integer observation times as

$$\theta^i_{k_n}=\theta^i_{k_0}+\sum_{j=1}^{n}\phi F(\mu^i_{k_{n-j}})e^{-\lambda j}. \tag{4}$$

This result facilitates the computation of the population-averaged firing threshold for population k at time step n

$$[\theta^i_{k_n}]=\theta_{k_n}=\theta_{k_0}+\sum_{j=1}^{n}\phi[F(\mu^i_{k_{n-j}})]e^{-\lambda j}.$$

Recalling that $F(\mu^i_k(t))\approx\sigma^i_k(t)$, we have that $[F(\mu^i_k(t))]\approx[\sigma^i_k(t)]=m_k(t)$. Therefore, we can rewrite the above as

$$\theta_{k_n}=\theta_{k_0}+\phi\sum_{j=1}^{n}m_{k_{n-j}}e^{-\lambda j}.$$

As the number of time-steps approaches infinity,

$$\lim_{n\to\infty}\theta_{k_n}=\theta_{k_\infty}=\theta_{k_0}+\lim_{n\to\infty}\phi\sum_{j=1}^{n}m_{k_{n-j}}e^{-\lambda j}. \tag{5}$$

Since for balanced dynamics we must have that $\lim_{n\to\infty}m_{k_n}=m_{k_\infty}$, Eq. (5) to leading order yields

$$\theta_{k_\infty}=\theta_{k_0}+\phi(m_{k_\infty}e^{-\lambda}+\ldots)=\theta_{k_0}+\phi\frac{m_{k_\infty}e^{-\lambda}}{1-e^{-\lambda}}. \tag{6}$$

Thus, Eq. (6) provides an analytical approximation for the long-time population-averaged firing threshold of utility in deriving parameter bounds for balanced dynamics in the next section.

In requiring that $0<m_k<1$, it is necessary for the time-averaged mean total input into each neuronal population to remain positive and finite, avoiding synchronous or completely quiescent network dynamics. For the kth population, the population-averaged total input, or mean total input, is

$$\begin{aligned}[\mu^i_k(t)]&=\left[\sum_{l=E,I}\sum_{j=1}^{N_l}R^{ij}_{kl}\sigma^j_l(t)+\mu^0_k-\theta^i_k(t)\right]\\&=\sum_{l=E,I}\sum_{j=1}^{N_l}[R^{ij}_{kl}][\sigma^j_l(t)]+\mu^0_k-[\theta^i_k(t)].\end{aligned}$$

Since each neuron is expected to receive K incoming connections of each type and the individual connection strength is $R_{kl}/\sqrt{K}$,

$$[\mu^i_k(t)]=\mu_k(t)=\sum_{l=E,I}R_{kl}\sqrt{K}m_l(t)+E_km_0\sqrt{K}-\theta_k(t). \tag{7}$$

Taking the time-average of the above expression over a long time horizon limit, such that $m_{k_\infty}\approx m_k$, yields

$$\mu_E=(Em_0+m_E-R_Em_I)\sqrt{K}-\theta_{E_\infty}, \tag{8a}$$

$$\mu_I=(Im_0+m_E-R_Im_I)\sqrt{K}-\theta_{I_\infty}. \tag{8b}$$

Hence, the long-time, time-averaged mean total excitatory and inhibitory inputs are at most $\mathcal{O}(\sqrt{K})$. The time-averaged mean inputs thus increase with network size yet must be dynamically adjusted in order for the network to exhibit asynchronous and irregular dynamics. It is therefore necessary for the total excitatory and total inhibitory inputs to approximately cancel for this to be possible in the large network limit, and so to yield $\mathcal{O}(1)$ mean inputs in the large network limit we require

$$Em_0 + m_E - R_E m_I - \frac{\theta_{E_\infty}}{\sqrt{K}} = \mathcal{O}(1/\sqrt{K}), \tag{9a}$$

$$Im_0 + m_E - R_I m_I - \frac{\theta_{I_\infty}}{\sqrt{K}} = \mathcal{O}(1/\sqrt{K}). \tag{9b}$$

Theoretical bounds on balanced dynamics

In deriving theoretical bounds on the network parameters which yield balanced dynamics, we consider two scenarios: (i) $\theta_{k_\infty} = o(\sqrt{K})$ and (ii) $\theta_{k_\infty} = \mathcal{O}(\sqrt{K})$ as $K \to \infty$ in the large network size limit. Case (i) corresponds to adaptation sufficiently small such that it has no impact on the time-averaged mean inputs in the large network size limit. Here standard balanced network theory holds (van Vreeswijk and Sompolinsky 1998), and the parameter bounds for balanced dynamics in both the excitatory and inhibitory populations are known to be

$$\frac{E}{I} > \frac{R_E}{R_I} > 1. \tag{10}$$

Thus, we focus case (ii), when $\theta_{k_\infty} = \mathcal{O}(\sqrt{K})$, to determine the impact of spike-frequency adaptation on the theoretical parameter bounds. According to Eq. (6), the long-time, population-averaged firing threshold θ_{k_∞} may only have an $\mathcal{O}(\sqrt{K})$ impact in Eq. (9) originating from the term $m_{k_\infty}\frac{\phi e^{-\lambda}}{1-e^{-\lambda}}/\sqrt{K}$, as the non-adapted threshold θ_{k_0} is assumed $\mathcal{O}(1)$. Requiring that Eq. (9) be satisfied when the *adaptation factor* $\omega = \frac{\phi e^{-\lambda}}{1-e^{-\lambda}}/\sqrt{K}$ is $\mathcal{O}(1)$ as $K \to \infty$ yields

$$Em_0 + (1-\omega)m_E - R_E m_I = \mathcal{O}(1/\sqrt{K}), \tag{11a}$$

$$Im_0 + m_E - (R_I + \omega)m_I = \mathcal{O}(1/\sqrt{K}). \tag{11b}$$

For K sufficiently large, this yields to leading order

$$\begin{bmatrix} 1-\omega & -R_E \\ 1 & -R_I - \omega \end{bmatrix} \begin{bmatrix} m_E \\ m_I \end{bmatrix} = \begin{bmatrix} -Em_0 \\ -Im_0 \end{bmatrix}.$$

with solution

$$m_E = \frac{(R_I+\omega)E - R_E I}{(R_I+\omega)(\omega-1) + R_E} m_0, \tag{12a}$$

$$m_I = \frac{E + (\omega-1)I}{(R_I+\omega)(\omega-1) + R_E} m_0. \tag{12b}$$

Requiring that both the excitatory and inhibitory populations are neither quiescent nor synchronous, in particular $0 < m_E < 1$ and $0 < m_I < 1$, we obtain parameter bounds

$$\frac{E}{I} > \frac{R_E}{R_I + \omega} > 1 - \omega > 0. \tag{13}$$

These new parameter bounds are especially illuminating when compared to the theoretical bounds obtained when spike-frequency adaptation is negligible given in Ineq. (10). First, note that adaptation factor ω is a monotonically increasing function of adaptation strength. Depending on the adaptation factor, qualitatively distinct dynamics manifest. We observe in Eq. (12) that the numerators of m_E and m_I are linearly monotonically increasing in ω and the common denominator is quadratically monotonically decreasing in ω for $\omega > (1 - R_I)/2$. Thus, for ω sufficiently large, the theoretical activities in both populations will decrease with adaptation strength. When adaptation strength is too large, the dynamics are expected to become unbalanced. For extremely strong adaptation, namely $\omega > 1$, we see from Eq. (8), increasing the theoretical mean excitatory population activity decreases the mean input into the excitatory population, thereby disrupting balance. Intuitively, as the adaptation strength becomes sufficiently large, the long-time firing threshold becomes of larger order than the expected inputs into each population, making balance impossible to sustain.

In contrast, for smaller ω, balanced dynamics can still be well reconciled with spike-frequency adaptation. For weak adaptation strength, $0 < \omega < 1 - R_I$, Eq. (12) demonstrates that adaptation instead *increases* the theoretical mean activity of each population. The effect of this can be seen in the adapted bounds given by Ineq. (13). In particular, for fixed R_I, the inequality holds for R_E larger in magnitude than in the non-adapted bounds in Ineq. (10). Intuitively, since $E > I$, the increase in m_E is more pronounced than the increase in m_I under weak adaptation, and thus the excitatory population may undergo additional recurrent inhibition and still maintain balanced dynamics.

For moderate adaptation strength, $1 - R_I < \omega < 1$, Ineq. (13) analogously implies that adaptation decreases the magnitude of the R_E for which balance holds for fixed R_I, implying that balance is maintained when the excitatory population is instead less recurrently inhibited. Here adaptation begins to *decrease* the mean activity of the two populations and, to compensate, more recurrent excitation is necessary to achieve non-adapted levels of activity in the balanced regime for the same choice of the remaining parameters.

We further observe that since $\frac{E}{I} > \frac{R_E}{R_I+\omega}$ in the adapted bounds, increasing the adaptation strength maintains balanced dynamics for potentially larger external inputs into the inhibitory population relative to a fixed external input into the excitatory population. Note that in the non-adapted case, increasing the external input into the excitatory population increases the theoretical mean activity of both populations and increasing the external input into the inhibitory population decreases the theoretical mean

activity in both populations. In contrast, based on the mean activities in Eq. (12) observed under adaptation, we see that if ω increases in the balanced regime, the decrease in theoretical activity garnered by increasing I is offset by ω, and thus a larger I is required to attain non-adapted levels of activity in the balanced regime for the same choice of the remaining parameters.

To provide additional intuition for the impact of adaptation strength on the model network dynamics, we contrast the network activity for two representative choices of adaptation parameters. For relatively weak adaptation strength, we observe, as depicted in Fig. 2a, typically any increases in threshold from firing events are mitigated by the decay in adaptation effect over time, yielding only a slight overall increase in spiking threshold. In Fig. 2b, we note that across both the excitatory and inhibitory populations, there is a small net gain in average threshold over a short time scale, leveling off to yield a nearly constant spiking threshold slightly increased relative to the non-adapted threshold. In this case, balance is still quite well maintained, with mean activities nearly constant about a slightly decreased value and EI ratios faintly elevated in magnitude, as shown in Fig. 2c, d. In contrast, when adaptation is sufficiently strong ($\omega > 1$), as considered analogously in Fig. 3, the mean spiking threshold increases significantly initially, ultimately saturating at a much larger value than in the case of more moderate adaptation. The level of mean activity decreases dramatically before saturating about a significantly smaller level of activity with a corresponding large increase in the magnitude of the EI ratios, indicating a severe loss in balance under extreme adaptation.

In light of these observations, we conclude that in the presence of weak or moderate adaptation, although the theoretical parameter bounds shift, balance is still achievable in the proper parameter regime. However, for strong adaptation, particularly $\omega > 1$, balance may no longer be achieved regardless of the choice of parameters. It is important to underline the fact that the case of strong adaptation is not biologically realistic (Benda and Herz 2003; La Camera et al. 2006; Augustin et al. 2013), and thus these theoretical considerations provide evidence that balanced dynamics may be reconciled with spike-frequency adaptation in physiological neuronal networks. We remark that our analysis does not make any specific assumptions about the relative number of excitatory and inhibitory neurons beyond $1 \ll K \ll N_E, N_I$, such that the neuronal populations are sufficiently large and sparsely connected for the mean-field limit to be well justified. Thus, balance may be consistent with spike-frequency adaptation in alternative regions of the brain with diverse ratios of excitatory to inhibitory neurons.

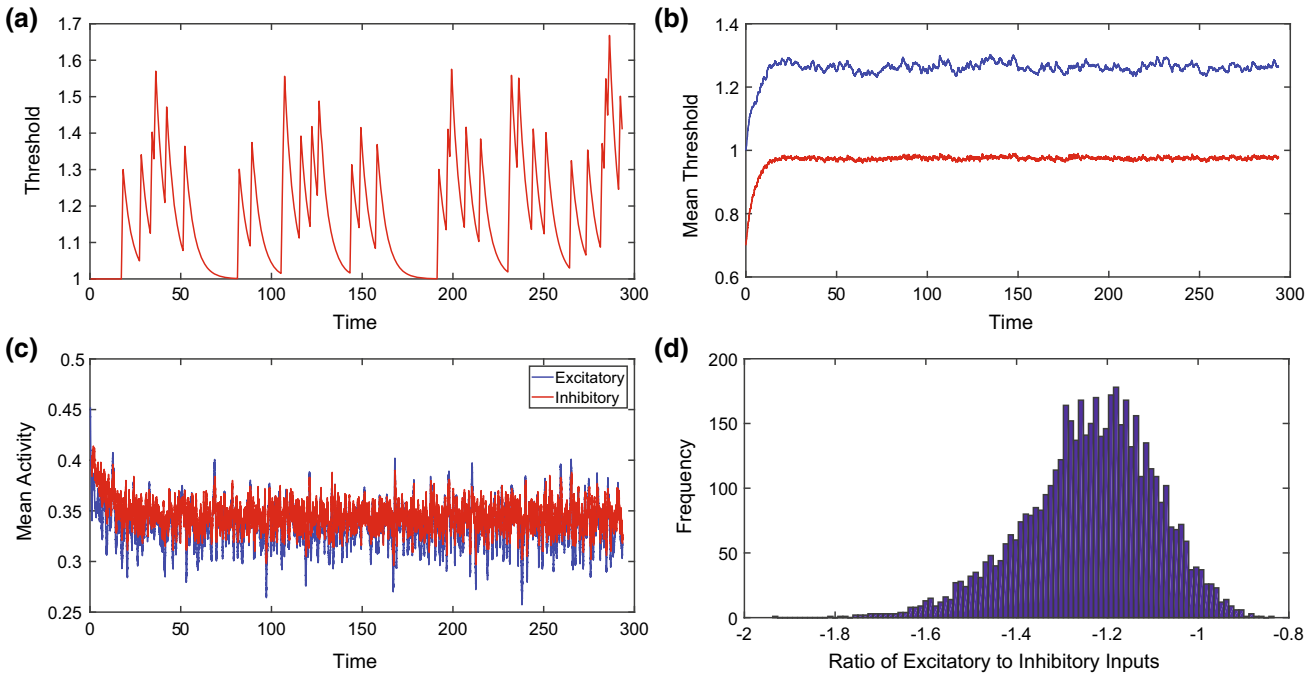

Fig. 2 Dynamics of binary neurons under moderate spike-frequency adaptation. **a** Firing threshold of a sample neuron over time. **b** Mean firing threshold across the excitatory (blue) and inhibitory (red) populations. **c** The mean activity across each neuron population. **d** Histogram of the ratio between time-averaged excitatory and inhibitory inputs across the neuronal network. Adaptation parameters are $\lambda = 0.2$ and $\phi = 0.3$, yielding adaptation factor $\omega < 1$. (Color figure online)

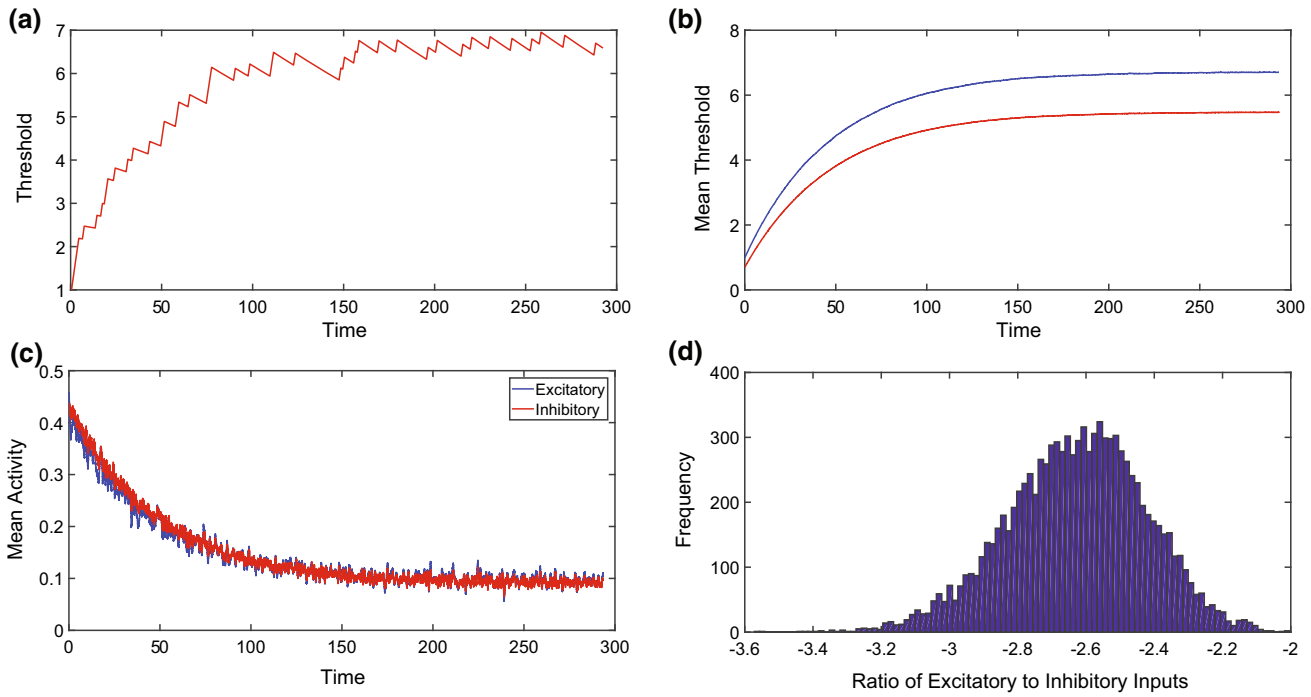

Fig. 3 Dynamics of binary neurons under strong spike-frequency adaptation. **a** Firing threshold of a sample neuron over time. **b** Mean firing threshold across the excitatory (blue) and inhibitory (red) populations. **c** The mean activity across each neuron population. **d** Histogram of the ratio between time-averaged excitatory and inhibitory inputs across the neuronal network. Adaptation parameters are $\lambda = 0.005$ and $\phi = 0.3$, yielding adaptation factor $\omega > 1$. (Color figure online)

Adaptation exclusively in excitatory population

Reflecting the physiological observation that excitatory neurons are typically more likely to undergo spike-frequency adaptation than inhibitory neurons (La Camera et al. 2006; Augustin et al. 2013), we instead assume that only the excitatory population is subject to adaptation. Significantly, the results in this case are fundamentally distinct from those obtained when both populations exhibit adaptation and provide valuable insights into a potentially new role of adaptation in cognition. Repeating the analysis in the previous section under the assumption $\theta_{I_\infty} = \theta_I$ yields

$$m_E = \frac{R_I E - R_E I}{R_I(\omega - 1) + R_E} m_0, \tag{14a}$$

$$m_I = \frac{E + (\omega - 1)I}{R_I(\omega - 1) + R_E} m_0 \tag{14b}$$

with corresponding parameter bounds

$$\frac{E}{I} > \frac{R_E}{R_I} > 1 - \omega. \tag{15}$$

We observe that when only the excitatory population is subject to adaptation, the parameter bounds necessary for balanced dynamics in fact *widen* with adaptation strength. As $\omega \to \infty$, Eq. (14) admits a solution such that $m_E \to 0$ and $m_I \to \frac{I}{R_I} m_0$, for which the inhibitory population never ceases firing, allowing the inhibitory population to exhibit asynchronous firing activity in response to the excitatory external input while the excitatory population is approximately quiescent. If we consider such a solution balanced, then $\omega > 1$ is an admissible parameter choice. In contrast, note that as $\omega \to \infty$ when both populations undergo adaptation, the firing rate for each population vanishes. Similar analysis demonstrates that in the case when only the inhibitory population undergoes spike-frequency attenuation, the parameter bounds for balance become more restrictive. For these reasons, we hypothesize that evolution may have selected for this network architecture, specifically adaptation primarily exhibited by excitatory neurons, with the goal of more robustly preserving balanced dynamics. We emphasize this holds broadly for alternative network parameters, reflecting diverse brain region structures, and thus may be a fundamental architectural principle aimed at robustly achieving balanced dynamics.

Numerical investigation of spike-frequency adaptation

The theoretical analysis discussed in the previous section held approximately in the large network limit. To discern the impact of spike-frequency adaptation for finite-sized neuronal networks and gain a more detailed perspective on the bounds on adaptation strength necessary for balanced dynamics, we exhaustively investigate the adaptation parameter space and its impact on several metrics of balance over an ensemble of network realizations. Performing analysis on a network of $N = 5000$ neurons, where all neurons undergo adaptation, we are able to provide a more detailed explanation of both when and how balance breaks down for sufficiently strong adaptation.

In Fig. 4, we vary adaptation jump strength ϕ and adaptation decay rate λ while holding the remainder of the model network parameters constant. First, we analyze the time-averaged mean ratio of the total excitatory and total inhibitory input into each neuron across the network in Fig. 4a. We observe that for weak adaptation (small ϕ and large λ), the mean EI ratio is close to -1, indicative of balance, with the EI ratio becoming more negative as the adaptation strength increases and the dynamics become more unbalanced. At the same time, as the adaptation strength increases, the time-averaged mean activities across the excitatory and inhibitory populations both decrease, as exhibited in Fig. 4b, c, respectively.

While it is clear balance breaks down for sufficiently strong adaptation, as the EI ratio decreases and mean activity across the network decreases, the precise mechanism for this transition in dynamics is important to discern. In Fig. 4d, e, we investigate the time-averaged mean total excitatory and inhibitory inputs, respectively, across the neuronal network. We note that while both types of input decrease in magnitude with adaptation strength, the decrease in the magnitude of the inhibitory input is significantly more dramatic. The mean firing threshold across the two populations increases comparably with adaptation, as shown in Fig. 4f, g, and thus the balance in EI ratio appears broken largely due to the disproportionate decrease in the magnitude of inhibitory inputs with high adaptation strength. Note that corresponding to this relatively large drop in the magnitude of the inhibitory input is a significant decrease in the mean activity of the inhibitory population, as shown in Fig. 4c, further evidencing that the inhibitory population is more strongly impacted by increased adaptation and thereby facilitates the breakdown in balanced dynamics.

These numerical results are consistent with the theoretical analysis in the previous sections. In particular, in Fig. 4h, we plot the adaptation factor $\omega = \frac{\phi e^{-\lambda}}{1-e^{-\lambda}}/\sqrt{K}$ over the adaptation parameterscape. We observe that for $\omega < 1$, when the long-time adapted threshold is expected to be of smaller size than the population inputs, the balanced operating regime is robust. Comparing the numerically computed value of the long-time population-averaged firing threshold to the theoretical approximation given by Eq. (6) for adaptation parameters in the balanced regime yields a relative error of only 0.07. Moreover, since the parameterscape plots in Fig. 4a–g closely mimic the changes in ω with λ and ϕ, the adaptation factor ω is indeed closely aligned with the degree of balance demonstrated by the network. Note that for the particular parameters numerically investigated, Ineq. (13) holds for $\omega < 1$, which is consistent with the choices of adaptation parameters empirically yielding balanced dynamics shown in Fig. 4a–g. It is important to remark that the rate at which the dynamics become unbalanced is quite slow for moderate attenuation strengths, with balance only rapidly diminishing for more extreme adaptation. Hence, even for networks of finite size, we see balanced dynamics are robust over a broad range of adaptation strengths.

Using the same choice of network parameters as discussed previously, we depict in Fig. 5 analogous metrics of balance for the more physiological case in which *only the excitatory population is subject to spike-frequency adaptation*. Here we see that the parameter regime in which balanced dynamics are preserved becomes significantly widened. Strikingly, there is only a marginal decrease in the mean EI ratio even for extreme choices of adaptation strength. In this case, the decrease in the time-averaged mean total excitatory and inhibitory inputs as well as mean activity are closely matched in magnitude, robustly preserving balance over the investigated parameterscape. Our numerical analysis thus agrees with the notion that by spike-frequency adaptation manifesting primarily in excitatory neurons, balanced dynamics are more broadly achieved over a larger space of network architectures and operating regimes than in the non-adapted case.

Generalization to integrate-and-fire model

To demonstrate that our results are generalizable to more physiological neuronal models with spike-frequency adaptation, we similarly investigate a pulse-coupled integrate-and-fire (I&F) network model (Corral et al. 1995; Mather et al. 2009; Barranca et al. 2014a). While relatively computationally inexpensive, the I&F model reproduces realistic neuronal firing rates and provides a fairly accurate description of physiological subthreshold voltage dynamics (Carandini et al. 1996; Rauch et al. 2003; Burkitt 2006).

We analyze two distinct variations of modeling spike-frequency adaptation in this framework. The first will

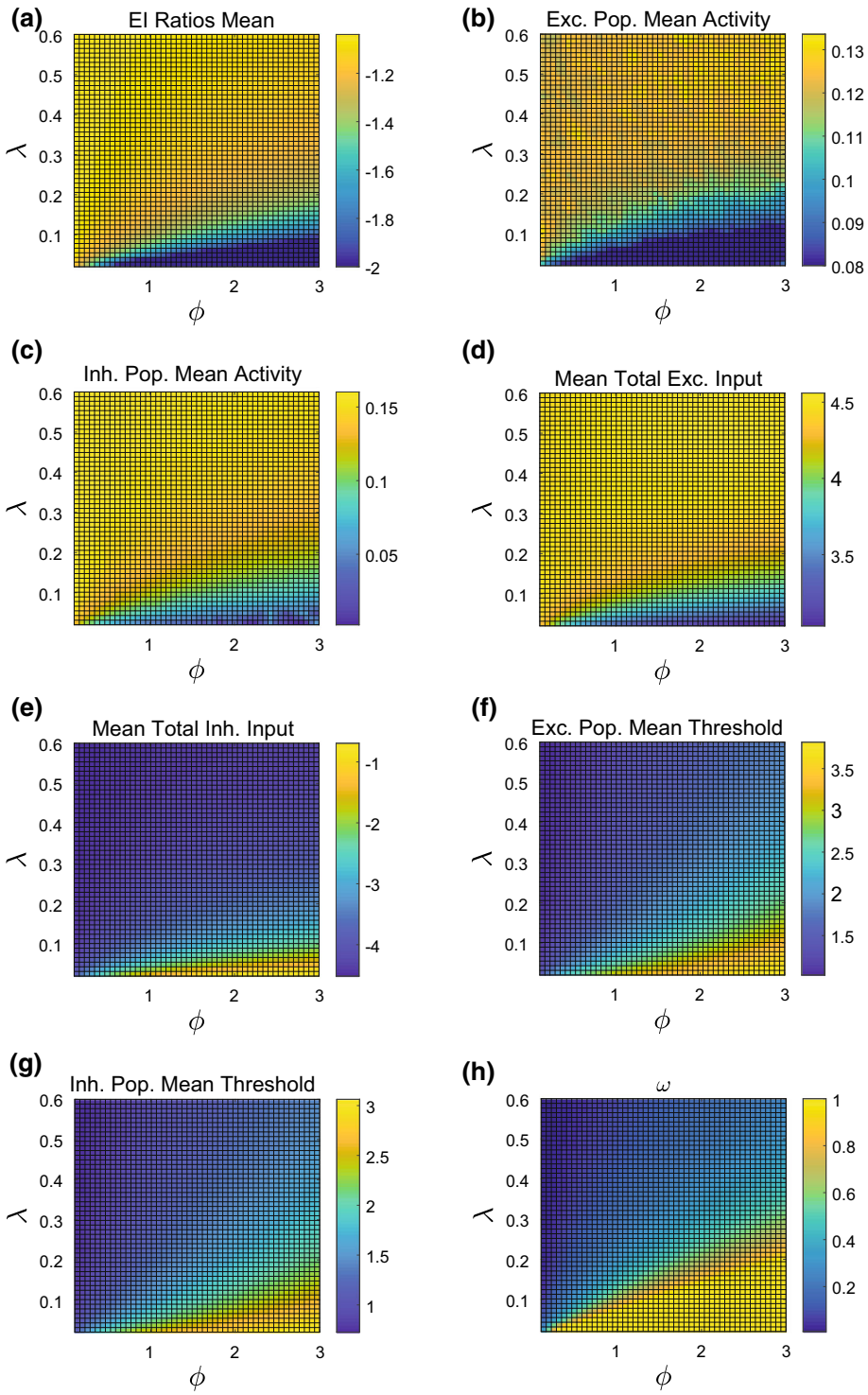

Fig. 4 Impact of adaptation strength on balanced dynamics when both the excitatory and inhibitory populations exhibit adaptation in a binary neuronal network. **a–f** Numerically investigate the effect of adaptation jump strength ϕ and adaptation decay rate λ on the: **a** mean ratio between time-averaged excitatory and inhibitory inputs across the neuronal network; **b** time-averaged mean activity of the excitatory neuron population; **c** time-averaged mean activity of the inhibitory neuron population; **d** time-averaged mean total excitatory input into the entire network; **e** time-averaged mean total inhibitory input into the entire network; **f** time-averaged mean firing threshold across the excitatory population; **g** time-averaged mean firing threshold across the inhibitory population; **h** adaptation factor $\omega = \frac{\phi e^{-\lambda}}{1-e^{-\lambda}}/\sqrt{K}$ thresholded at $\omega = 1$

model adaptation analogously to the binary case by increasing the neuronal firing threshold for each neuron after it undergoes a firing event. The second will instead keep the firing threshold constant while explicitly including an adaptation current that decreases firing rate following action potentials.

The membrane-potential dynamics of the ith neuron in kth population of the pulse-coupled I&F network, v_k^i, is modeled by the differential equation

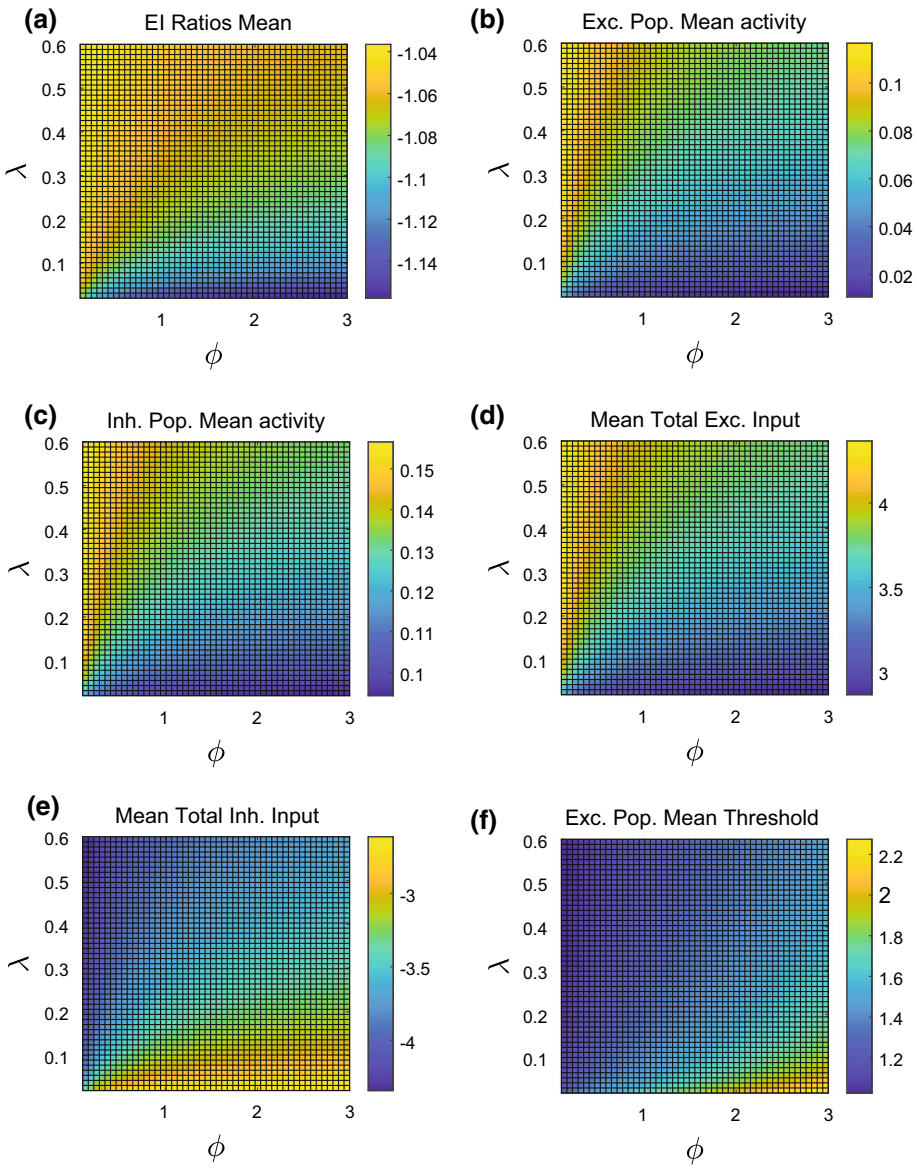

Fig. 5 Impact of adaptation strength on balanced dynamics when *only the excitatory population exhibits adaptation* in a binary neuronal network. **a**–**f** Numerically investigate the effect of adaptation jump strength ϕ and adaptation decay rate λ on the: **a** mean ratio between the time-averaged excitatory and inhibitory inputs across the neuronal network; **b** time-averaged mean activity of the excitatory neuron population; **c** time-averaged mean activity of the inhibitory neuron population; **d** time-averaged mean total excitatory input into the entire network; **e** time-averaged mean total inhibitory input into the entire network; **f** time-averaged mean firing threshold across the excitatory population

$$\tau \frac{dv_k^i}{dt} = -\left(v_k^i - \theta_k^i\right) + u_k^0 + \sum_{\substack{j=1 \\ j\neq i}}^{N_E} R_{kE}^{ij} \sum_l \delta(t - \tau_{jl}^E) + \sum_{\substack{j=1 \\ j\neq i}}^{N_I} R_{kI}^{ij} \sum_l \delta(t - \tau_{jl}^I), \tag{16}$$

evolving continuously on a time-scale reflected by τ, until reaching firing threshold θ_k^i. At that moment the neuron is said to fire and its state is instantaneously reset to the value v_R. Using the same notation and connectivity structure as in the binary model, a neuron in the kth population receives external input u_k^0 and the realization of adjacency matrix, R, determines the recurrent connectivity in the network. Neuronal interactions are reflected at the moment of action potentials such that at the time of the lth firing event of the jth neuron in the kth population, τ_{jl}^k, the activity of all post-connected neurons is offset as a result of integrating over the Dirac delta function $\delta(\cdot)$ in Eq. (16).

For an identical choice of network architecture parameters as considered for the binary model in Fig. 1, we briefly underline several aspects of the dynamics of the I&F network in the balanced regime. As shown in Fig. 6a, the ratio of the time-averaged excitatory and inhibitory inputs across the network is clustered near -1, indicative of balance. The mean activity for each population across time is nearly constant, depicted in Fig. 6b, demonstrating neither synchronous nor quiescent dynamics overall. This asynchronous activity is also reflected in the raster plot shown in Fig. 6c, which exhibits a sequence of points corresponding to the index of each spiking neuron as a function of the time of each action potential.

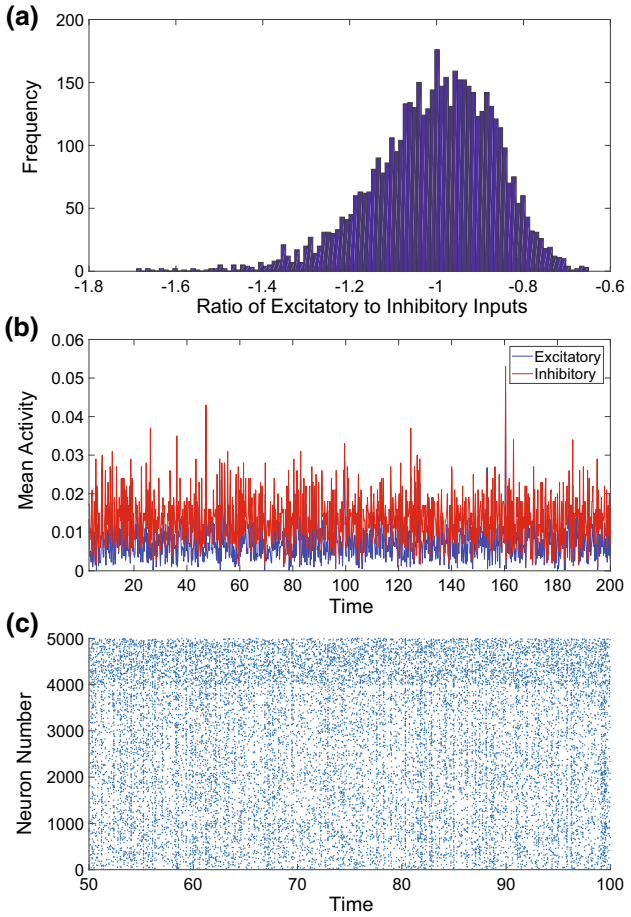

Fig. 6 Dynamics of integrate-and-fire neurons in the balanced operating regime. **a** Histogram of the ratio between time-averaged excitatory and inhibitory inputs across the neuronal network. **b** The mean activity across the excitatory (blue) and inhibitory (red) populations. **c** Raster plot displaying asynchronous firing activity across the network, displayed for a subset of simulation time for greater resolution. The network architecture is identical to the binary network considered in Fig. 1. (Color figure online)

Using first an I&F model with *threshold-based* adaptation, we reflect spike-frequency adaptation by increasing the firing threshold of the ith neuron in the kth population, $\theta_k^i(t)$, by ϕ the moment the neuron fires. Between firing events, $\theta_k^i(t)$, evolves according to

$$\frac{d\theta_k^i}{dt} = -\lambda(\theta_k^i - \theta_k), \tag{17}$$

such that the firing threshold decays to the constant non-adapted firing threshold for all neurons in the kth population, θ_k, in the absence of firing events. Hence, analogous to the binary model with adaptation, ϕ determines the instantaneous increase in threshold following a firing event and λ determines the decay rate of the threshold offset.

Reflecting the essential characteristics of more biologically realistic adaptation currents, we also analyze an I&F model with *current-based* adaptation, which specifically incorporates an adaptation current $w_k^i(t)$ associated with the ith neuron in the kth population while instead keeping the firing threshold constant at θ_k. The dynamical system model is adjusted in this case to

$$\tau\frac{dv_k^i}{dt} = -(v_k^i - \theta_k) + u_k^0 + \sum_{\substack{j=1\\ j\neq i}}^{N_E} R_{kE}^{ij}\sum_l \delta(t-\tau_{jl}^E) + \sum_{\substack{j=1\\ j\neq i}}^{N_I} R_{kI}^{ij}\sum_l \delta(t-\tau_{jl}^I) - w_k^i$$

$$\frac{dw_k^i}{dt} = -\lambda w_k^i, \tag{18}$$

where w_k^i is instantaneously increased by ϕ at each time its corresponding neuron fires and λ controls the decay rate for the adaptation current.

In generalizing our analysis to the framework of the I&F model, it is important to note that in the absence of adaptation, neurons in the balanced operating regime asynchronously fire at a low rate and their spike trains are approximately independent. Thus, the summed spike train input of each type into each neuron tends asymptotically towards a Poisson spike process (Cinlar 1972). In effect, the mean network drive from the kth population to a neuron in the jth population is approximately $m_k R_{jk}\sqrt{K}$. For this reason, the balance condition for the pulse-coupled I&F network model is identical to Ineq. (10) derived for the binary network model. In addition, the cumulative impact of firing events on the firing threshold $\theta_k^i(t)$ for a given neuron in the threshold-based I&F model is given by $\phi\sum_{\tau_{il}^k} e^{-\lambda(t-\tau_{il}^k)}$, which is the continuous analog for the increase in threshold corresponding to firing events in the adapted binary model. The analysis in the "Mean-field analysis" section therefore carries over approximately to the I&F network with threshold-based adaptation and yields a perturbed adaptation factor that agrees with ω to leading order. Ineq. (13) thus retains an identical structure and dependence on the resultant adaptation factor, thereby demonstrating a similar theoretical relationship between adaptation strength and balanced activity. Following in suite, we expect that the bounds for balanced dynamics determined for the I&F model with current-based adaptation at least qualitatively demonstrates the same structure as the adapted binary model and confirm this numerically.

We underline the numerical evidence that our previous binary model analysis naturally generalizes to the I&F model in Fig. 7, thereby providing a more robust connection between balanced dynamics and adaptation. In Fig. 7a, b, we plot the time-averaged mean EI ratio and time-averaged mean threshold, respectively, across the I&F

network with threshold-based adaptation over the $\lambda - \phi$ parameter space. We see a nearly identical structure as observed in the binary network, with the EI ratio decreasing for sufficiently high adaptation strength and high corresponding mean spiking threshold. Likewise, in Fig. 7c, d, we depict analogous plots for the I&F network with current-based adaptation, which demonstrate the same trend. If instead only the excitatory population undergoes spike-frequency attenuation, we observe in Fig. 7e, f that both versions of the adapted I&F network demonstrate little deviation from balance in the EI ratio even under high adaptation strengths, agreeing with the notion that adaptation facilitates balanced dynamics in this case.

Discussion

Our work demonstrates in the context of several neuronal network models that balanced dynamics are well preserved for physiological spike-frequency adaptation strengths. We verify this theoretically in the large network limit and provide detailed numerical evidence in the finite network case. While for sufficiently strong adaptation, balance does diminish, such strengths are inconsistent with what is observed in vivo. In the case when only excitatory neurons undergo adaptation, as found in many areas of the brain, we show that balance is yet more robustly preserved over a wide parameter space. This provides new evidence for the hypothesis that neuronal networks may have evolved such

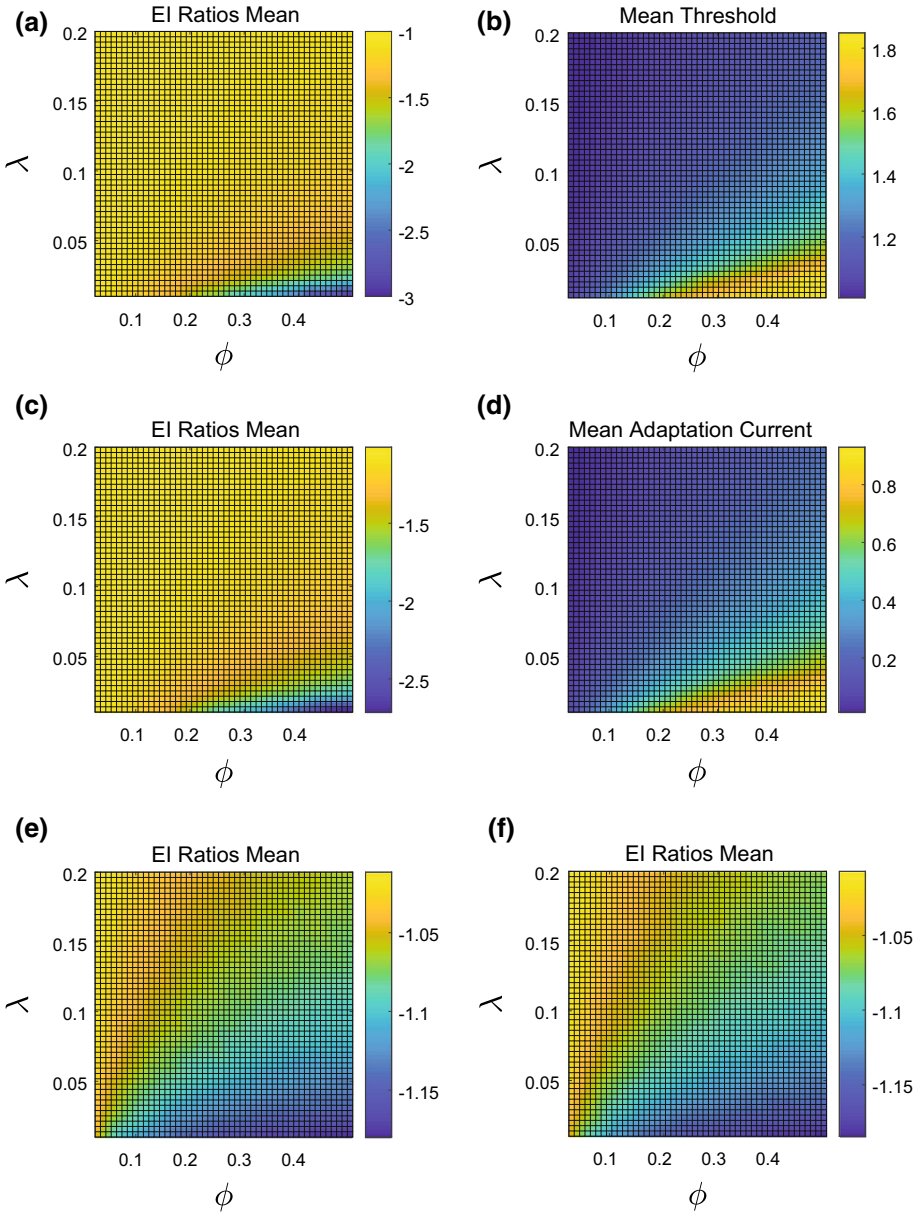

Fig. 7 Impact of adaptation strength on balanced dynamics in integrate-and-fire networks. Each panel numerically investigates the effect of adaptation jump strength ϕ and adaptation decay rate λ. **a** Mean ratio between time-averaged excitatory and inhibitory inputs across a neuronal network in which all neurons undergo threshold-based adaptation. **b** Time-averaged mean firing threshold across a neuronal network in which all neurons undergo threshold-based adaptation. **c** Mean ratio between time-averaged excitatory and inhibitory inputs across a neuronal network in which all neurons undergo current-based adaptation. **d** Time-averaged adaptation current w across a neuronal network in which all neurons undergo current-based adaptation. **e** Mean ratio between time-averaged excitatory and inhibitory inputs across a neuronal network in which only excitatory neurons undergo threshold-based adaptation. **f** Mean ratio between time-averaged excitatory and inhibitory inputs across a neuronal network in which only excitatory neurons undergo current-based adaptation

that excitatory neurons exhibit spike attenuation in order to maintain balanced dynamics over a broad range of operating states, potentially improving input encoding and memory.

There are numerous lines of experimental evidence suggesting that an imbalance in inhibitory and excitatory neuronal inputs may underlie autism spectrum disorders as well as schizophrenia (Gao and Penzes 2015; Tatti et al. 2017; Nelson and Valakh 2015; Rosenberg et al. 2015), and thus degeneracies in neuronal dynamics, such as particularly strong or weak adaptation, could potentially aid in explaining disorders in brain function. It may therefore be informative to further examine experimentally the link between adaptation and balanced dynamics.

While we investigated the relationship between spike-frequency adaptation and the balanced operating regime in the context of the binary and integrate-and-fire neuronal models, we expect that our framework for investigation largely generalizes to more physiological network models with slow adaptation currents incorporated, such as the Hodgkin-Huxley model and the quadratic as well as exponential integrate-and-fire neuronal models (Richardson 2009; Fourcaud-Trocme et al. 2003; Barranca et al. 2014a). As the theory of balanced networks for continuous models has largely been developed for pulse-coupled neuronal networks (Boerlin et al. 2013; Litwin-Kumar and Doiron 2012; Mongillo et al. 2012; Renart et al. 2010; Deneve and Machens 2016), we expect that studying alternative neuronal models with pulse-coupling would facilitate the most natural setting to extend the results of this study. Though we investigated the impact of several idealized models of spike-frequency attenuation in this work, in light of the multitude of alternative models and mechanisms for spike-frequency adaptation (Barranca et al. 2014a; Treves 1993; Liu and Wang 2001; Smith et al. 2002; Mensi et al. 2012; Touboul and Brette 2008), analogously studying adaptation in more physiological forms would make for an interesting area of future examination. Our theoretical analysis was more tractable under the assumption that the network connectivity was homogeneous and random; however, an important direction for future study is the impact of adaptation on the balanced operating regime in networks with more biologically realistic structure, such as a small-world or scale-free architecture, commonly observed in the brain (Dorogovtsev and Mendes 2002; van den Heuvel et al. 2008; Sporns and Honey 2006; Netoff et al. 2004; Roxin et al. 2004).

Funding Funding was provided by National Science Foundation (Grant No. DMS-1812478) and Swarthmore College (Faculty Research Support Grant).

References

Achard S, Bullmore E (2007) Efficiency and cost of economical brain functional networks. PLoS Comput Biol 3(2):e17

Atallah BV, Scanziani M (2009) Instantaneous modulation of gamma oscillation frequency by balancing excitation with inhibition. Neuron 62(4):566–577

Augustin M, Ladenbauer J, Obermayer K (2013) How adaptation shapes spike rate oscillations in recurrent neuronal networks. Front Comput Neurosci 7:9

Barranca VJ, Johnson DC, Moyher JL, Sauppe JP, Shkarayev MS, Kovačič G, Cai D (2014a) Dynamics of the exponential integrate-and-fire model with slow currents and adaptation. J Comput Neurosci 37(1):161–180

Barranca VJ, Kovačič G, Zhou D, Cai D (2014b) Sparsity and compressed coding in sensory systems. PLoS Comput Biol 10(8):e1003793

Benda J, Herz AV (2003) A universal model for spike-frequency adaptation. Neural Comput 15(11):2523–2564

Benda J, Longtin A, Maler L (2005) Spike-frequency adaptation separates transient communication signals from background oscillations. J Neurosci 25(9):2312–2321

Benda J, Maler L, Longtin A (2010) Linear versus nonlinear signal transmission in neuron models with adaptation currents or dynamic thresholds. J Neurophysiol 104(5):2806–2820

Bibikov NG, Ivanitski GA (1985) Simulation of spontaneous discharge and short-term adaptation in acoustic nerve fibers. Biofizika 30(1):141–144

Boerlin M, Machens CK, Deneve S (2013) Predictive coding of dynamical variables in balanced spiking networks. PLoS Comput Biol 9(11):e1003258

Britten KH, Shadlen MN, Newsome WT, Movshon JA (1993) Responses of neurons in macaque MT to stochastic motion signals. Vis Neurosci 10(6):1157–1169

Brown DA, Adams PR (1980) Muscarinic suppression of a novel voltage-sensitive K+ current in a vertebrate neurone. Nature 283(5748):673–676

Burkitt AN (2006) A review of the integrate-and-fire neuron model: I. Homogeneous synaptic input. Biol Cybern 95(1):1–19. ISSN 0340-1200 (Print). https://doi.org/10.1007/s00422-006-0068-6

Carandini M, Mechler F, Leonard CS, Movshon JA (1996) Spike train encoding by regular-spiking cells of the visual cortex. J Neurophysiol 76(5):3425–3441. Nov ISSN 0022-3077 (Print); 0022-3077 (Linking)

Chacron MJ, Longtin A, St-Hilaire M, Maler L (2000) Suprathreshold stochastic firing dynamics with memory in P-type electroreceptors. Phys Rev Lett 85(7):1576–1579

Cinlar E (1972) Superposition of point processes. In: Lewis PAW (ed) Stochastic point processes: statistical analysis, theory, and applications. Wiley, New York, pp 549–606

Compte A, Constantinidis C, Tegner J, Raghavachari S, Chafee MV, Goldman-Rakic PS, Wang XJ (2003) Temporally irregular mnemonic persistent activity in prefrontal neurons of monkeys during a delayed response task. J Neurophysiol 90(5):3441–3454

Corral Á, Pérez CJ, Díaz-Guilera A, Arenas A (1995) Self-organized criticality and synchronization in a lattice model of integrate-and-fire oscillators. Phys Rev Lett 74(1):118–121. Jan ISSN 0031-9007

Deneve S, Machens CK (2016) Efficient codes and balanced networks. Nat Neurosci 19(3):375–382

Destexhe A, Rudolph M, Pare D (2003) The high-conductance state of neocortical neurons in vivo. Nat Rev Neurosci 4(9):739–751

Dorogovtsev SN, Mendes JFF (2002) Evolution of networks. Adv Phys 51:1079–1187

Ermentrout B, Pascal M, Gutkin B (2001) The effects of spike frequency adaptation and negative feedback on the synchronization of neural oscillators. Neural Comput 13(6):1285–1310. June ISSN 0899-7667 (Print); 0899-7667 (Linking)

Faisal AA, Selen LP, Wolpert DM (2008) Noise in the nervous system. Nat Rev Neurosci 9(4):292–303

Fourcaud-Trocme N, Hansel D, van Vreeswijk C, Brunel N (2003) How spike generation mechanisms determine the neuronal response to fluctuating inputs. J Neurosci 23(37):11628–11640. ISSN 1529-2401 (Electronic)

Gao R, Penzes P (2015) Common mechanisms of excitatory and inhibitory imbalance in schizophrenia and autism spectrum disorders. Curr Mol Med 15(2):146–167

Gilbert CD (1992) Horizontal integration and cortical dynamics. Neuron 9(1):1–13

Glauber RJ (1963) Time-dependent statistics of the ising model. J Math Phys 4(2):294–307

He Y, Chen ZJ, Evans AC (2007) Small-world anatomical networks in the human brain revealed by cortical thickness from MRI. Cereb Cortex 17(10):2407–2419

Kilpatrick ZP, Ermentrout B (2011) Sparse gamma rhythms arising through clustering in adapting neuronal networks. PLoS Comput Biol 7(11):e1002281

Kobayashi R (2009) The influence of firing mechanisms on gain modulation. J Stat Mech Theory Exp 2009(01):P01017

Kobayashi R, Kitano K (2016) Impact of slow k+ currents on spike generation can be described by an adaptive threshold model. J Comput Neurosci 40(3):347–362

La Camera G, Rauch A, Thurbon D, Luscher HR, Senn W, Fusi S (2006) Multiple time scales of temporal response in pyramidal and fast spiking cortical neurons. J Neurophysiol 96(6):3448–3464

Litwin-Kumar A, Doiron B (2012) Slow dynamics and high variability in balanced cortical networks with clustered connections. Nat Neurosci 15(11):1498–1505

Liu G (2004) Local structural balance and functional interaction of excitatory and inhibitory synapses in hippocampal dendrites. Nat Neurosci 7(4):373–379

Liu YH, Wang XJ (2001) Spike-frequency adaptation of a generalized leaky integrate-and-fire model neuron. J Comput Neurosci 10(1):25–45

London M, Roth A, Beeren L, Hausser M, Latham PE (2010) Sensitivity to perturbations in vivo implies high noise and suggests rate coding in cortex. Nature 466(7302):123–127

Markram H, Lubke J, Frotscher M, Roth A, Sakmann B (1997) Physiology and anatomy of synaptic connections between thick tufted pyramidal neurones in the developing rat neocortex. J Physiol 500 (Pt 2):409–440. April ISSN 0022-3751 (Print); 0022-3751 (Linking)

Mason A, Nicoll A, Stratford K (1991) Synaptic transmission between individual pyramidal neurons of the rat visual cortex in vitro. J Neurosci 11(1):72–84

Mather W, Bennett MR, Hasty J, Tsimring LS (2009) Delay-induced degrade-and-fire oscillations in small genetic circuits. Phys Rev Lett 102(6):068105

Mensi S, Naud R, Pozzorini C, Avermann M, Petersen CC, Gerstner W (2012) Parameter extraction and classification of three cortical neuron types reveals two distinct adaptation mechanisms. J Neurophysiol 107(6):1756–1775

Miura K, Tsubo Y, Okada M, Fukai T (2007) Balanced excitatory and inhibitory inputs to cortical neurons decouple firing irregularity from rate modulations. J Neurosci 27(50):13802–13812

Mongillo G, Hansel D, van Vreeswijk C (2012) Bistability and spatiotemporal irregularity in neuronal networks with nonlinear synaptic transmission. Phys Rev Lett 108(15):158101

Nelson SB, Valakh V (2015) Excitatory/inhibitory balance and circuit homeostasis in autism spectrum disorders. Neuron 87(4):684–698

Netoff TI, Clewley R, Arno S, Keck T, White JA (2004) Epilepsy in small-world networks. J Neurosci 24(37):8075–8083. Sept ISSN 1529-2401 (Electronic); 0270-6474 (Linking). https://doi.org/10.1523/JNEUROSCI.1509-04.2004

Peron S, Gabbiani F (2009) Spike frequency adaptation mediates looming stimulus selectivity in a collision-detecting neuron. Nat Neurosci 12(3):318–326

Rauch A, La Camera G, Luscher H-R, Senn W, Fusi S (2003) Neocortical pyramidal cells respond as integrate-and-fire neurons to in vivo-like input currents. J Neurophysiol 90(3):1598–1612. Sept ISSN 0022-3077 (Print); 0022-3077 (Linking). https://doi.org/10.1152/jn.00293.2003

Renart A, de la Rocha J, Bartho P, Hollender L, Parga N, Reyes A, Harris KD (2010) The asynchronous state in cortical circuits. Science 327(5965):587–590

Richardson MJE (2009) Dynamics of populations and networks of neurons with voltage-activated and calcium-activated currents. Phys Rev E 80(2):021928

Rosenberg A, Patterson JS, Angelaki DE (2015) A computational perspective on autism. Proc Natl Acad Sci USA 112(30):9158–9165

Roxin A, Riecke H, Solla SA (2004) Self-sustained activity in a small-world network of excitable neurons. Phys Rev Lett 92:198101. https://doi.org/10.1103/PhysRevLett.92.198101

Shadlen MN, Newsome WT (1998a) The variable discharge of cortical neurons: implications for connectivity, computation, and information coding. J Neurosci 18(10):3870–3896

Shadlen MN, Newsome WT (1998b) The variable discharge of cortical neurons: implications for connectivity, computation and information coding. J Neurosci 18:3870–3896

Shu Y, Hasenstaub A, McCormick DA (2003) Turning on and off recurrent balanced cortical activity. Nature 423(6937):288–293

Smith GD, Cox CL, Sherman SM, Rinzel J (2002) A firing-rate model of spike-frequency adaptation in sinusoidally-driven thalamocortical relay neurons. Thalamus Relat Struct 1:135–156

Softky WR, Koch C (1993) The highly irregular firing of cortical cells is inconsistent with temporal integration of random EPSPs. J Neurosci 13(1):334–350

Sporns O, Honey CJ (2006) Small worlds inside big brains. Proc Natl Acad Sci USA 103(51):19219–19220. Dec ISSN 0027-8424 (Print); 0027-8424 (Linking). https://doi.org/10.1073/pnas.0609523103

Stiefel KM, Gutkin BS, Sejnowski TJ (2009) The effects of cholinergic neuromodulation on neuronal phase-response curves of modeled cortical neurons. J Comput Neurosci 26(2):289–301

Sussillo D, Abbott LF (2009) Generating coherent patterns of activity from chaotic neural networks. Neuron 63(4):544–557

Tatti R, Haley MS, Swanson OK, Tselha T, Maffei A (2017) Neurophysiology and Regulation of the Balance Between Excitation and Inhibition in Neocortical Circuits. Biol Psychiatry 81(10):821–831

Touboul J, Brette R (2008) Dynamics and bifurcations of the adaptive exponential integrate-and-fire model. Biol Cybern 99(4–5):319–334. Nov ISSN 1432-0770 (Electronic); 0340-1200 (Linking). https://doi.org/10.1007/s00422-008-0267-4

Treves A (1993) Mean-field analysis of neuronal spike dynamics. Netw Comput Neural Syst 4(3):259–284

Troyer TW, Miller KD (1997) Physiological gain leads to high ISI variability in a simple model of a cortical regular spiking cell. Neural Comput 9(5):971–983

van den Heuvel MP, Stam CJ, Boersma M, Hulshoff Pol HE (2008) Small-world and scale-free organization of voxel-based resting-

state functional connectivity in the human brain. Neuroimage 43(3):528–539. Nov ISSN 1095-9572 (Electronic); 1053-8119 (Linking). https://doi.org/10.1016/j.neuroimage.2008.08.010

van Vreeswijk C, Hansel D (2001) Patterns of synchrony in neural networks with spike adaptation. Neural Comput 13(5):959–992

van Vreeswijk C, Sompolinsky H (1996) Chaos in neuronal networks with balanced excitatory and inhibitory activity. Science 274:1724–1726

van Vreeswijk C, Sompolinsky H (1998) Chaotic balanced state in a model of cortical circuits. Neural Comput 15:1321–1371

Vogels TP, Abbott LF (2005) Signal propagation and logic gating in networks of integrate-and-fire neurons. J Neurosci 25:10786–95

Wehr M, Zador AM (2003) Balanced inhibition underlies tuning and sharpens spike timing in auditory cortex. Nature 426(6965):442–446

Whalley K (2013) Neural coding: timing is key in the olfactory system. Nat Rev Neurosci 14(7):458

Xue M, Atallah BV, Scanziani M (2014) Equalizing excitation-inhibition ratios across visual cortical neurons. Nature 511(7511):596–600

Yamada W, Koch C, Adams P (1989) Multiple channels and calcium dynamics. In: Methods in neuronal modeling: from synapses to networks, pp 97–133. MIT Press